Available online at www.sciencedirect.com
ScienceDirect
Journal of the European Ceramic Society 27 (2007) 351–356
www.elsevier.com/locate/jeurceramsoc

Effects of residual stresses on the fracture properties of non-oxide laminated composites

S. Guicciardi [a,c], M. Nagliati [a,c], C. Melandri [a,c], G. Pezzotti [b,c], D. Sciti [a,c,*]

[a] CNR-ISTEC, Institute of Science and Technology for Ceramics, Via Granarolo 64, I-48018 Faenza, Italy
[b] Department of Chemistry and Materials Technology, Kyoto Institute of Technology, Sakyo-ku, Matsugasaki, 606-8585 Kyoto, Japan
[c] Research Institute for Nanoscience (RIN), Kyoto Institute of Technology, Sakyo-ku, Matsugasaki, 606-8585 Kyoto, Japan

Received 16 November 2005; received in revised form 26 April 2006; accepted 29 April 2006
Available online 16 June 2006

Abstract

A layered ceramic composite in the AlN–SiC–$MoSi_2$ system was prepared with the outer layers under residual compressive stress. The mechanical properties of the constituent layers and of the laminated composite were measured. Due to the residual compressive stress, the fracture strength of the laminated composite was higher than the strength of the outer layer material. The fracture toughness of the laminar composite was evaluated by SEVNB. The resulting values were compared with a fracture mechanics model and a good agreement was found between the experimental measurements and the calculated apparent fracture toughness profile.

Keyword: Composites; Mechanical properties; Laminates; AlN; SiC; $MoSi_2$

1. Introduction

The design of ceramic laminates has been proved to be a viable strategy to obtain significant increases of the fracture resistance of ceramic materials.[1–7] The basic idea is to couple material layers with different thermal expansion coefficients (CTE) so that residual stresses arise during cooling from the sintering temperature. The relative thickness of adjacent layers, their Young's modulus and CTEs affect these residual stresses whose sign and magnitude can be adjusted through the composition, the stacking sequence and the layer thicknesses.

Compressive layers placed within a laminate have been proved to be able to arrest cracks and this phenomenon can produce composites with a threshold strength in which failure does not occur until a critical stress is applied.[8] Also the fracture toughness benefits from the presence of compressive layers across laminated composites.[9,10] Moreover, residual surface compressive stresses have been shown to improve the tribological properties.[11]

In this work, a non-oxide ceramic multilayer was produced by the tape casting technique. The layered composite was obtained by alternating layers with two different compositions in the AlN–SiC–$MoSi_2$ system and with a stacking sequence that left the outer layers under compression. AlN–SiC–$MoSi_2$ ceramic composites were previously shown to couple good mechanical properties to electro-conductivity.[12–14] In similar compositions and architecture, these composites are currently employed in industrial applications such as heaters and igniters. It is therefore mandatory from the engineering point of view to understand the effects of the residual stresses on the mechanical properties of the layered architecture, with particular emphasis on the fracture properties. To this purpose, in the present paper mechanical properties of the constituent materials and of the layered composite were measured and analysed.

2. Experimental

2.1. Materials preparation

Two different layers with the following compositions (in vol.%) were prepared:

- $55AlN + 15SiC + 30MoSi_2$, labelled as C;
- $80AlN + 10SiC + 10MoSi_2$, labelled as I.

* Corresponding author. Tel.: +39 0546 699 748; fax: +39 0546 46381.
E-mail address: dile@istec.cnr.it (D. Sciti).

0955-2219/$ – see front matter © 2006 Elsevier Ltd. All rights reserved.
doi:10.1016/j.jeurceramsoc.2006.04.173

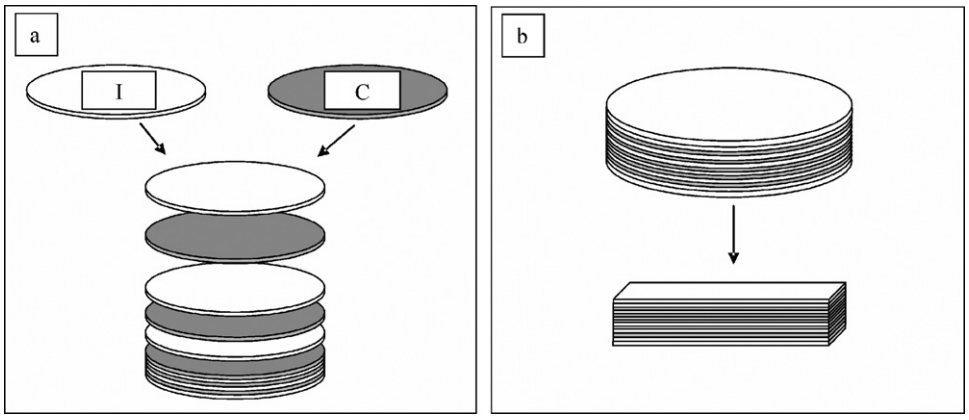

Fig. 1. (a) Schematic diagram of the multilayer preparation and (b) bars preparation.

Circular samples with thickness of 250 μm and diameter of 40 mm were punched out from the as-cast green tapes. Both monolithic and layered samples were produced. Monolithic samples were prepared by individually stacking I or C layers. The layered samples were produced by stacking 21 layers with sequence I/I/C/I. . .I/C/I/I. A schematic diagram is presented in Fig. 1. All the laminate materials, composite and monolithic, were warm-pressed at 75 °C for 15 min with an applied pressure of 17 MPa, and then heated at 80 °C for 15 min without pressure. The burnout stage (150 °C/h from 25 to 600 °C, 30 min holding time) was followed by sintering in a graphite furnace (1850 °C/30 min) under flowing nitrogen. More details of the processing are reported in Refs.[15,16]

The relative densities of the sintered samples were measured by Archimede's method. On the polished cross section of the samples, the microstructure was analysed by scanning electron microscopy (SEM, Cambridge S360) and energy dispersive microanalysis (EDS, INCA Energy 300, Oxford instruments, UK). The linear thermal expansion coefficient (CTE) of the monolithic materials was measured with dilatometric tests (Netzsch Geraetebau Dil E 402, Germany) up to 1400 °C in air, with a heating rate of 5 °C/min. The Young's modulus (E) of the monolithic materials was measured by the resonance frequency method on 28 mm × 8 mm × 0.8 mm specimens using an H&P gain-phase analyzer. The flexural strength (σ) of the monolithic materials and the laminated composite was measured on a 4-pt bending fixture (outer span: 20 mm, inner span: 10 mm) with a crosshead speed of 0.5 mm/min using chamfered bars 25 mm × 2.50 mm × 1.75 mm, length × width × thickness, respectively. The fracture toughness of the monolithic materials and laminated composite was measured by Single Edge V-Notched Beam (SEVNB). From the laminated composite, bars of about 25 mm × 4 mm × 3 mm (length × thickness × width) were cut with the bar thickness corresponding to the thickness of the sintered disc, as shown in Fig. 1b. A notch was first introduced at the centre of the bending bar with a 500 μm-thick diamond saw, then this notch was sharpened using a razor blade sprinkled with 3 μm diamond paste. Care was taken in positioning the notch tip well within a tensile or compressive layer, Fig. 2. The notched bars were fractured in a 3-pt bending device with a crosshead of 0.5 mm/min and the apparent fracture toughness, K_{Ic}, was calculated according to the SENB formula:[17]

$$K_{Ic} = \frac{P_c S}{BW^{3/2}} f(\alpha) \quad (1)$$

where

$$f(\alpha) = \frac{3\alpha^{1/2}[1.99 - \alpha(1-\alpha)(2.15 - 3.93\alpha + 2.7\alpha^2)]}{2(1+2\alpha)(1-\alpha)^{3/2}} \quad (2)$$

P_c is the critical load at fracture, S the span, B the width of the bar, W the thickness of the bar and α the ratio between notch length (a) and bar thickness W.

3. Results and discussion

3.1. Microstructure of the materials

The relative density of the laminate composite after sintering was about 98%. A very good adhesion was found between the layers as visible delamination or large structural defects at the interface were not found. A polished cross section of the

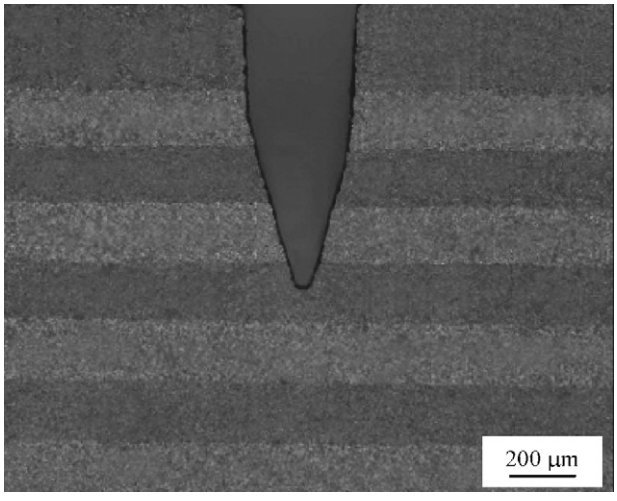

Fig. 2. Optical micrograph showing an example of the notch introduced in the 21-layers bars.

multilayer composite is shown in Fig. 3a. The layers' thickness was in the range of 170–200 μm. Small variations in thickness were unavoidable since the discs were produced from different tapes with the same compositions. In Fig. 3b and c, detailed views of the single layers are reported. A small amount of porosity was found in both layers (∼1–2%). Further details on the microstructure are reported elsewhere.[16] The monolithic materials presented similar microstructural features. No trace of the junction between the stacked layers was found, such that these specimens resembled bulk materials.

3.2. Properties of the monolithic materials

Some properties of the monolithic materials are reported in Table 1. The CTEs were linear function of the temperature in the measured range. The CTE of material C was higher than that of material I, due to the higher content of $MoSi_2$, which is the phase with the highest CTE. Typical values reported in the literature for the pure phases are:[18] AlN: $5.59 \times 10^{-6}\,^{\circ}C^{-1}$, SiC: $5.12 \times 10^{-6}\,^{\circ}C^{-1}$, $MoSi_2$: $9.1 \times 10^{-6}\,^{\circ}C^{-1}$.

The higher value of Young's modulus of material C is mainly due to the higher amount of $MoSi_2$ and SiC, which are very stiff phases (∼440 GPa[18]).

The fracture toughness of material C was higher than that of material I (Table 1), very likely as a result of the higher content of $MoSi_2$. Due to its high value of CTE, the higher content of $MoSi_2$ increased the residual stress in the AlN–SiC matrix, which acted as a toughening mechanism.[19]

The flexural strength of both materials was relatively high with a low dispersion around the mean value, see Table 1. Material I was slightly stronger than material C.

3.3. Calculation of the residual stresses in the laminated composite

The residual stresses in the various rigidly bonded layers can be estimated according to the lamination theory:[3]

$$\varepsilon_i = \frac{1-\nu_i}{E_i}\sigma_i + \alpha_i \Delta T = \text{constant} \quad (3)$$

$$\sum_i \sigma_i t_i = 0 \quad (4)$$

where ε_i is the elastic residual deformation and σ_i the stress developed in the layer of thickness t_i. Respectively, α_i, E_i and ν_i are the thermal expansion coefficient, the Young's modulus and the Poisson's ratio of layer i. ΔT is the temperature-range over which elastic stress develops due to thermal strain mismatch.

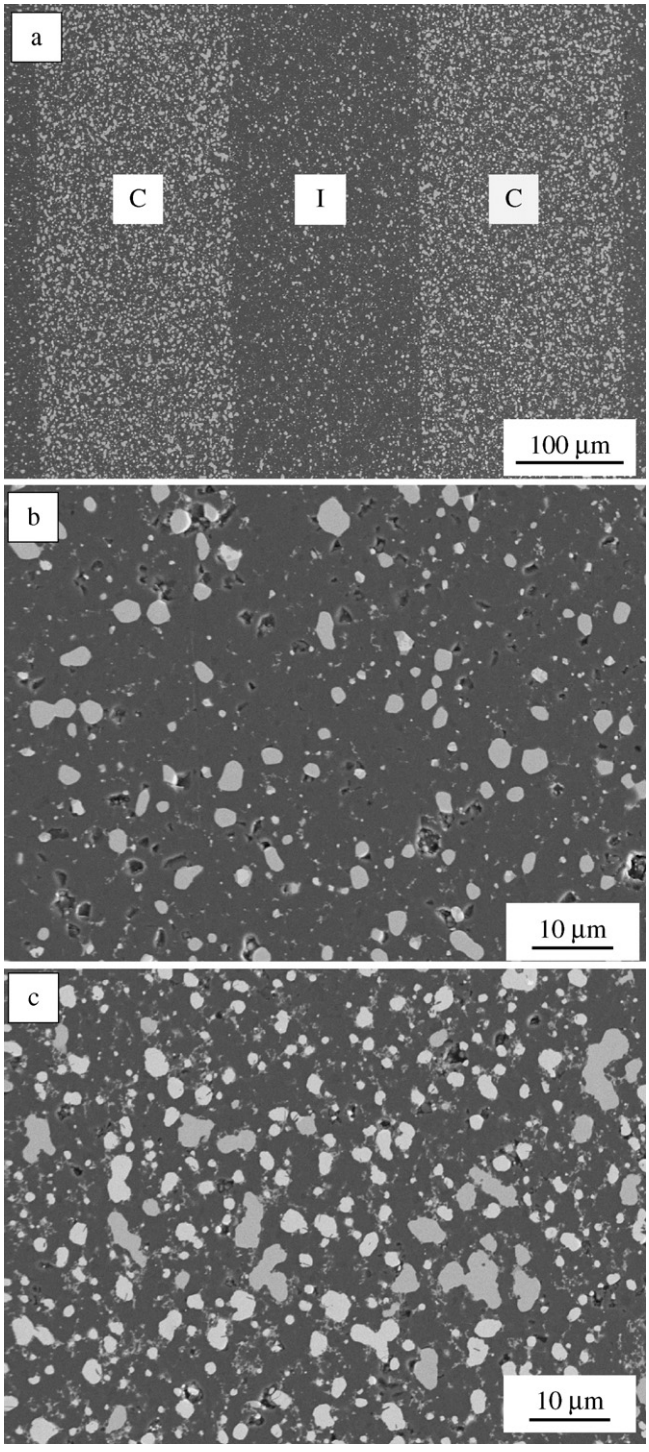

Fig. 3. SEM micrographs of the microstructure of the multilayer samples. (a) Panoramic view of the layered material. (b) Detailed view of the I layer, and (c) of the C layer. The $MoSi_2$ phase is visible as bright contrast grains dispersed in the AlN–SiC matrix.

Table 1
Compositions and properties of the constituent materials

Material	Composition (vol.%)	E (GPa)	ν	CTE (25–1000 °C) ($\times 10^{-6}$/°C)	K_{Ic} (MPa m$^{0.5}$)	σ (MPa)
I	80AlN + 10SiC + 10$MoSi_2$	325	0.27	6.20	2.1 ± 0.1	571 ± 25
C	55AlN + 15SiC + 30$MoSi_2$	348	0.23	6.87	2.8 ± 0.4	513 ± 23

Apparent fracture toughness and flexural strength of the laminated composite material. E = Young's modulus, ν = Poisson's ratio (calculated), CTE = linear thermal expansion coefficient, K_{Ic} = fracture toughness, σ = 4-pt bending strength.

For the calculations, the Poisson's ratios of the different layers were determined with the rule of mixture on the basis of the starting compositions and are 0.27 and 0.25 for the I and C materials, respectively, while the α_i, and E_i values were taken as those experimentally determined (Table 1). A crucial parameter for the calculation with theoretical models is the stress-free temperature, i.e. the temperature below which stresses are accumulated elastically. This stress-free temperature is difficult to determine experimentally and is usually taken to be somewhat lower than the sintering temperature, with 1200 °C being a quite common choice. In a recent study[10] temperatures as low as 675 °C were selected in order to get a good agreement with theoretical and experimental results. However, in the present case, the temperature was selected a priori considering that each individual layer contains $MoSi_2$ for which a brittle-to-ductile transition occurs at about 1000 °C.[20] Taking 1000 °C as stress-free temperature, the calculated residual stresses were −123 MPa (compressive) in the insulating I layers and +146 MPa (tensile) in the conductive C layers for the 21-layers specimens produced for toughness measurements.

3.4. Properties of the laminated composite

3.4.1. Flexural strength

The flexural strength of the laminated composite, calculated on seven specimens, was 622 ± 41 MPa with minimum and maximum values of 574 and 694 MPa, respectively. No evidence of stable crack growth was observed in any of the load–displacement curves. The values of flexural strength were calculated considering the stress field across the section of the bending bar with a stepwise Young's modulus profile, i.e.:[21,22]

$$\sigma_{\text{flex}}(x) = \frac{P(S_{\text{out}} - S_{\text{inn}})}{4B} E'(x) \frac{E_2 - E_1 x}{E_2^2 - E_1 E_3} \tag{5}$$

where P is the applied load, S_{out} and S_{inn} the outer and inner span, respectively, B the width of the bar and $E'(x)$ the in-depth plain strain variation of the Young's modulus across the section of the laminated bar. The expressions of E_1, E_2 and E_3 are the following:

$$E_1 = \int_0^W E'(x)\,\mathrm{d}x \tag{6}$$

$$E_2 = \int_0^W xE'(x)\,\mathrm{d}x \tag{7}$$

$$E_3 = \int_0^W x^2 E'(x)\,\mathrm{d}x \tag{8}$$

For the construction of the Young's modulus profile, the thickness of each individual layer was measured in every single bar. Since in bending the highest tensile stress is located at the tensile external surfaces, the strength of the laminated composite is mainly dictated by the outer layer strength. The outer layer of the laminated composite was made of material I which, in its stress-free state, had a mean flexural strength of 571 MPa (Table 1). Therefore, due to the residual compressive stress originating from the lamination processing, the increase in strength of this material in the laminated composite was about 50 MPa. This value is of the same order of magnitude of the compressive residual stress calculated by the lamination theory even if lower. The non-perfect match between these two values is due to the fact that in some fractured bars the fracture origins were not located in the external layer. An example of this situation is shown in Fig. 4a and b.

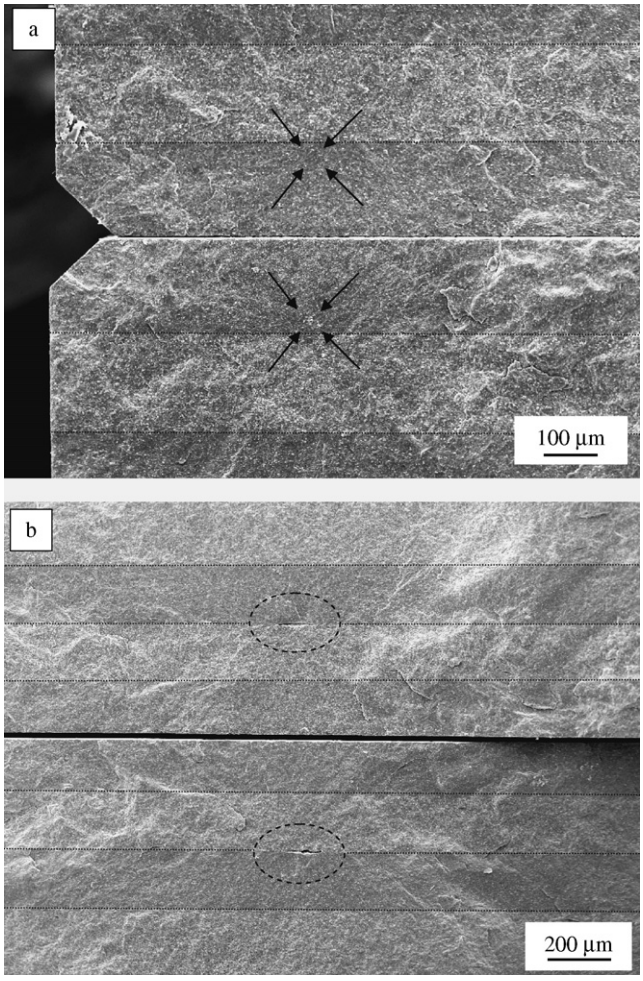

Fig. 4. Examples of fracture origins of the laminated bars (SEM micrographs). (a) An inhomogeneity located in the external layer, flexural strength = 694 MPa. (b) Large microcrack at the interface between the second and the third layer, flexural strength = 574 MPa.

3.4.2. Fracture toughness

The apparent fracture toughness of the laminated composite was in the range of 3.8–5.6 MPa $m^{0.5}$. During the tests, neither pop-in phenomena or stable crack propagation were detected when the notch tip was located either in the compressive layer or in the tensile layer. The apparent fracture toughness values were therefore calculated considering the crack length a as the initial notch depth. Even if not particularly large, the data dispersion of the apparent fracture toughness is the main outcome of the different stress profiles, which exists along the notches with different depths. In fact, the measured apparent fracture toughness is the result of the superposition of the externally applied flexural stress and the residual stress profile inside the laminate

structure.[23] By fracture mechanics analysis, the effects of the stress field superposition can be estimated by considering that the stress-intensity factor, K_I, of a crack of length a due to an arbitrary distribution of crack-line stress $\sigma(x)$ is

$$K_I = \int_0^a h\left(\frac{x}{a}, \alpha\right) \sigma(x)\, dx \quad (9)$$

where $h(x/a, \alpha)$ is a weight function given by[23]

$$h\left(\frac{x}{a}, \alpha\right) = \sqrt{\frac{2}{\pi a}} \frac{1}{(1-(x/a))^{1/2}(1-\alpha)^{3/2}} \times \left\{(1-\alpha)^{3/2} + \sum A_{ij}\left(1-\frac{x}{a}\right)^{i+1}\alpha^j\right\} \quad (10)$$

and α is the crack length normalized for the bar thickness (a/W). The in-depth stress distribution $\sigma(x)$ in a laminated bar of thickness W and width B subjected to 3-pt bending over a span of S is given by[21]

$$\sigma(x) = \sigma_{flex}(x) + \sigma_r(x) \quad (11)$$

where $\sigma_{flex}(x)$ is given by Eq. (5) and $\sigma_r(x)$ is the residual stress at point x given by

$$\sigma_r(x) = \sigma_1 \quad \text{for } x \text{ corresponding to the I layers}$$
$$(-123\ \text{MPa, in the present case})$$
$$= \sigma_2 \quad \text{for } x \text{ corresponding to the C layers}$$
$$(+146\ \text{MPa, in the present case})$$

For the calculations of the apparent fracture toughness profile, the coefficients A_{ij} in Eq. (6) were taken from Ref.[24], which considered the case of a flexural bar made of a homogeneous material without variation of Young's modulus across its section. However, as shown in Ref.,[25] even with a strong gradient profile of Young's modulus across the section of the bar, the difference in the calculated stress intensity factor remains <10%. The apparent fracture toughness profile of the laminated composite was calculated as follows.[23] For any crack length a, a corresponding critical bending load, P_c, was calculated so that, integrating Eq. (9) with the stress distribution given by Eq. (11), the intrinsic (i.e. stress-free) K_{Ic} for the material containing the tip of the crack a was obtained. This couple (a, P_c) was then inserted in Eqs. (1) and (2) to find out the corresponding apparent fracture toughness. By varying the crack length and the corresponding P_c, the apparent fracture toughness profile as a function of crack length a can be drawn. In order to obtain a unique K_{Ic} profile, the thickness of the layers were in this case averaged. This apparent K_{Ic} profile is shown in Fig. 5 along with the experimental data points. As can be seen, the apparent K_{Ic} is an increasing function of the crack length in the compressive layer and a decreasing function of the crack length in the tensile layer with values ranging from 0.9 to 7.2 MPa m$^{0.5}$. Recognising all the approximations involved in the calculation of the apparent fracture toughness, the agreement between the theoretical curve and the experimental points can be considered quite good.

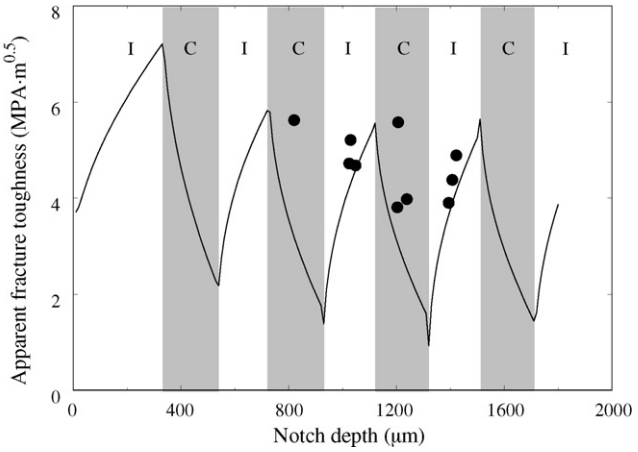

Fig. 5. Apparent fracture toughness profile and superimposition of experimental data points.

4. Conclusions

A layered ceramic composite in the AlN–SiC–$MoSi_2$ system was prepared by tape-casting. The composite was prepared by alternatively stacking electrical insulating and conductive laminae. The stacking was such that the outer layers were under residual compressive stress. The magnitude of the residual stresses was estimated through the lamination theory. The mechanical properties of the constituent materials and the layered composite were measured. With respect to the stress-free outer material, the fracture strength of the laminated composite increased by an amount comparable to the compressive residual stress calculated by the lamination theory. The apparent fracture toughness of the laminated composite was estimated by an analytical fracture mechanics model and a good agreement was found between experimental values and the predictions of fracture mechanics.

References

1. Marshall, D. B., Ratto, J. J. and Lange, F. F., Enhanced fracture toughness in layered microcomposites of Ce–ZrO_2 and Al_2O_3. *J. Am. Ceram. Soc.*, 1991, **74**, 2979–2987.
2. Sathyamoorthy, R., Virkar, A. V. and Cutler, R. A., Damage-resistant SiC–AlN layered composites with surface compressive stresses. *J. Am. Ceram. Soc.*, 1992, **75**, 1136–1141.
3. Chartier, T., Merle, D. and Besson, J. L., Laminar ceramic composites. *J. Eur. Ceram. Soc.*, 1995, **15**, 101–107.
4. Šajgalík, P., Lenčeš, Z. and Dusza, J., Layered Si_3N_4 composites with enhanced room temperature properties. *J. Mater. Sci.*, 1996, **31**, 4837–4842.
5. Rao, M. P., Sánchez-Herencia, A. J., Beltz, G. E., McMeeking, R. M. and Lange, F. F., Laminar ceramics that exhibit a threshold strength. *Science*, 1998, **286**, 102–105.
6. Kovar, D., Thouless, M. D. and Halloran, J. W., Crack deflection and propagation in layered silicon nitride/boron nitride ceramics. *J. Am. Ceram. Soc.*, 1998, **81**, 1004–1012.
7. Cai, P. Z., Green, D. J. and Messing, G. L., Mechanical characterization of Al_2O_3/ZrO_2 hybrid laminates. *J. Eur. Ceram. Soc.*, 1998, **5**, 2025–2034.
8. Rao, M. P. and Lange, F. F., Factors affecting threshold strength in laminar ceramic containing thin compressive layers. *J. Am. Ceram. Soc.*, 2002, **85**, 1222–1228.
9. Blattner, A. J., Lakshminarayanan, R. and Shetty, D. K., Toughening of layered ceramic composites with residual surface compression: effects of layer thcickness. *Eng. Fract. Mech.*, 2001, **68**, 1–7.

10. Lugovy, M., Slyunyayev, V., Orlovskaya, N., Blugan, G., Kuebler, J. and Lewis, M., Apparent fracture toughness of Si_3N_4-based laminates with residual compressive or tensile stresses in surface layers. *Acta Mater.*, 2005, **53**, 289–296.
11. Toschi, F., Melandri, C., Pinasco, P., Roncari, E., Guicciardi, S. and De Portu, G., Influence of residual stress on the wear behaviour of alumina/alumina zirconia laminated composites. *J. Am. Ceram. Soc.*, 2003, **86**, 1543–1547.
12. Sciti, D., Guicciardi, S., Melandri, C. and Bellosi, A., High-temperature resistant composites in the AlN–SiC–$MoSi_2$ system. *J. Am. Ceram. Soc.*, 2003, **86**, 1720–1726.
13. Sciti, D. and Guicciardi, S., Microstructure and mechanical properties of novel ternary electroconductive ceramics. *J. Mat. Res.*, 2004, **19**, 3343–3352.
14. Krnel, K., Sciti, D. and Bellosi, A., Influence of long-term oxidation on the microstructure, mechanical and electrical properties of pressureless sintered AlN–SiC–$MoSi_2$ ceramic composites. *J. Eur. Ceram. Soc.*, 2003, **23**, 3135–3146.
15. Roncari, E., Pinasco, P., Nagliati, M. and Sciti, D., Tape casting of AlN–SiC–$MoSi_2$ composites. *J. Eur. Ceram. Soc.*, 2004, **24**, 2303–2311.
16. Sciti, D., Nagliati, M., Tochino, S., Pezzotti, G. and Guicciardi, S., Fabrication and residual stresses characterization of novel non-oxide multilayer ceramics. *J. Eur. Ceram. Soc.*, in press.
17. ASTM E-399-83, Standard test method for plain-strain fracture toughness of metallic material. *Annual book of ASTM standards, Section 3, Metals test methods and analytical procedures*. American Society for Testing and Materials, Philadelphia, PA, 1984, pp. 519–554.
18. Shackelford, J. F. and Alexander, W., ed., *CRC Materials science and engineering handbook*. CRC Press, Boca Raton, FL, 2001.
19. Taya, M., Hayashi, S., Kobayashi, A. S. and Yoon, H. S., Toughening of a particulate-reinforced ceramic-matrix composite by thermal residual stress. *J. Am. Ceram. Soc.*, 1990, **73**, 1382–1391.
20. Jang, Y.-L. and Lavernia, E. J., Review, Processing of Molybdenum Disilicide. *J. Mat. Sci.*, 1994, **29**, 2557–2571.
21. Moon, R. J., Hoffman, M., Hilden, J., Bowman, K. J., Trumble, K. P. and Rodel, J., Weight function analysis on the *R*-curve behavior of multilayered alumina–zirconia composites. *J. Am. Ceram. Soc.*, 2002, **85**, 1505–1511.
22. Moon, R. J., Hoffman, M., Hilden, J., Bowman, K. J., Trumble, K. P. and Rodel, J., *R*-curve behavior in alumina–zirconia composites with repeating graded layers. *Eng. Fract. Mech.*, 2002, **69**, 1647–1665.
23. Lakshminarayanan, R., Shetty, D. K. and Cutler, R. A., Toughening of layered ceramic composites with residual surface compression. *J. Am. Ceram. Soc.*, 1996, **79**, 79–87.
24. Fett, T. and Munz, D., Influence of crack–surface interactions on stress intensity factor in ceramics. *J. Mater. Sci. Lett.*, 1990, **9**, 1403–1406.
25. Fett, T., Munz, D. and Yang, Y. Y., Applicability of the extended Petroski-Achenbach weight function procedure to graded materials. *Eng. Fract. Mech.*, 2000, **65**, 393–403.